UCRL-91970
PREPRINT

THE 14 MeV NEUTRON WORK AT THE LAWRENCE LIVERMORE NATIONAL LABORATORY

Luisa F. Hansen

University of California
Lawrence Livermore National Laboratory
Livermore, CA 94550

This paper was prepared for submittal to
The International Symposium on Fast Neutrons
in Science and Technology
February 4-9, 1985
Chiang Mai, Thailand

July 1985

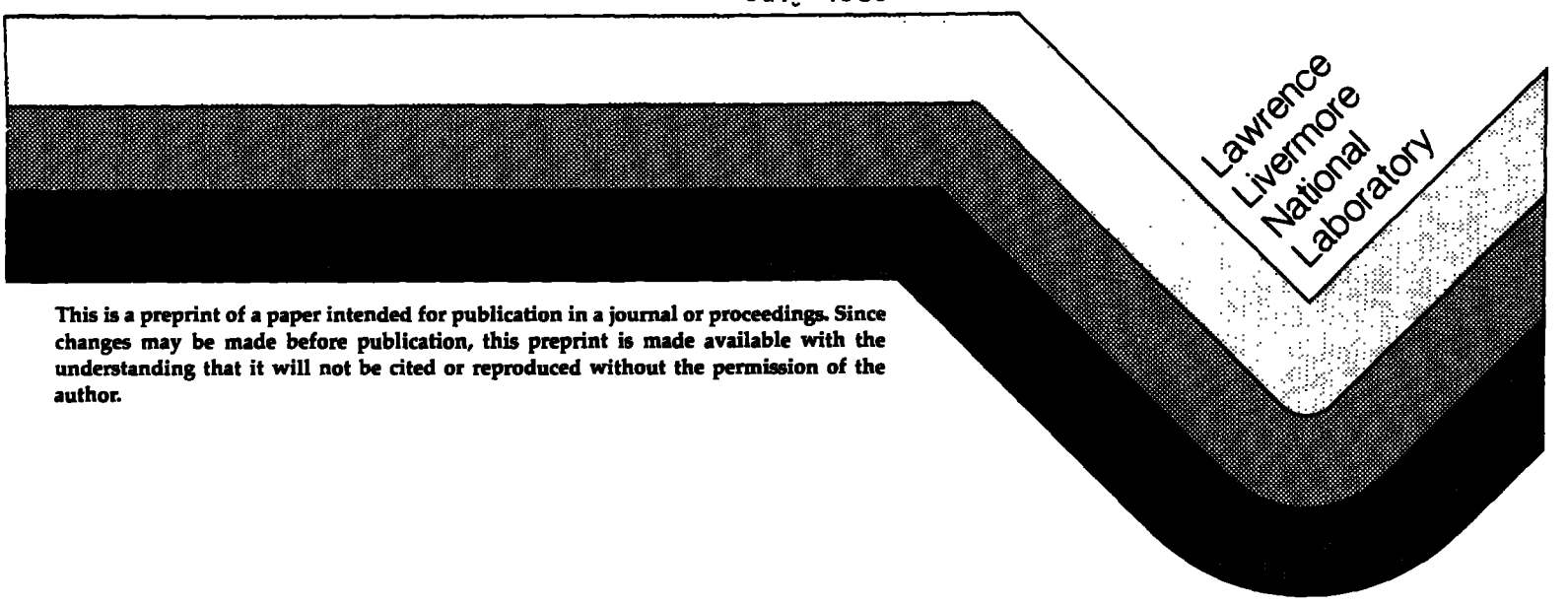

DISCLAIMER

THE 14 MeV NEUTRON WORK AT THE LAWRENCE LIVERMORE NATIONAL LABORATORY

L. F. Hansen

Lawrence Livermore National Laboratory
University of California
Livermore, California 94550

ABSTRACT

The 14 MeV neutron work at Lawrence Livermore National Laboratory (LLNL) covers two main areas of interest to this Symposium: 1) measurements and calculations of differential cross sections, and 2) integral measurements of the neutron and gamma emission spectra. In both areas a large number of materials have been studied, spanning a wide mass range ($6 < A < 239$), of interest to fusion and hybrid reactors. In this presentation a brief description of the experimental techniques and calculational analysis is given for each of the above areas and the measured and calculated cross sections are discussed.

DIFFERENTIAL NEUTRON MEASUREMENTS

OBJECTIVE

A large body of elastic differential cross sections measurements has been published in the last therty years[1] for materials ranging from hydrogen to uranium. However, these measurements and their analysis have been carried under quite different conditions of beam energy resolution, size and geometry of the targets, flight paths, detector efficiency, and multiple scattering

correction for large targets. This lack of uniformity which accounts for the wide variations observed in the quality of the published data was our main incentive to carry out these measurements at Livermore. We were also interested in assessing the value of microscopic optical potentials, such as the Jeukenne, Lejeune, and Mahaux (JLM)[2] and Brieva and Rook (BR)[3] potentials, as a tool to predict neutron differential cross sections. This test required a consistent set of measurements over a wide mass and energy range. In this paper the measurements of the angular distributions will be dicussed for the elastic scattering of 14.6 MeV neutrons from ^{9}Be, C, ^{27}Al, Fe, ^{59}Co, ^{89}Y, ^{93}Nb, In, ^{140}Ce, ^{181}Ta, ^{197}Au, ^{208}Pb, ^{209}Bi. For ^{232}Th, ^{238}U and ^{239}Pu the angular distributions were measured at 14.1 MeV.

MEASUREMENTS

The measurements have been made using as a 14.6 MeV neutron source the ^{2}H(d,n)^{3}He reaction at 0° using the 12 MeV incident deuteron beam from the LLNL tandem electrostatic accelerator. The beam is bunched, 1-2 ns wide, and swept at a 2.5 MHz burst rate. The deuterium target is a 1 cm diameter by 3 cm long gas cell filled to a pressure of 2 atm. Details on the target fabrication can be found elsewhere[4]. Two identical cells mounted on their respective parallel stems can rotate into position in the deuterium beam path are used during the measurements. One cell is filled to 2 atm of deuterium and the second one is evacuated in order to measure the neutron background contribution from the empty cell. The zero degree 14.6 neutron burst impinged on the scattering samples positioned at 20 cm from the gas cell. The targets, Be, C, Al, Fe, Co, Y, Nb, In, ^{140}Ce, Ta, Au, ^{208}Pb, and Bi, are cylinders of 2.5 cm diameter and 5 cm height. They are mounted on a hollow 1 cm

diameter nylon pole whose contribution to the background is negligible because of its very small mass.

The scattered neutrons are detected using the LLNL time-of-flight (TOF) facility[5] in which 16 NE213 liquid scintillator detectors (11.3 cm diameter by 5.1 cm long) allow simultaneous measurements in the angular region 3.5° to 159°. In the present work the elastic angular distributions have been measured between 9.2° and 159° with a 10.75 m flight path for all the detectors. The 3.5° detector turned off during the scattering run is used to measure the incident flux on the scatterer. The detector bias is 5.4 MeV and pulse shape discrimination is used to reduce the gamma-ray background. Figure 1 shows a schematic view of the TOF facility. Details on the experimental technique and analysis of the data can be found in Ref. 1.

OPTICAL MODEL ANALYSIS OF THE DATA

A. Microscopic calculations. The microscopic optical potentials[2,3] (MOP) contain the central and spin-orbit potentials which include the direct and exchange terms. The central potentials are calculated by folding integrals of an effective interaction g(r) between the projectile and target nucleons with the nuclear density. The exchange terms are calculated by carrying a suitable local momentum approximation of g(r).

$$U(r_1) = \int \rho(r_2) g(r) d^3 r_2 \qquad (1)$$

where r_1 and r_2 refer to the projectile and target nucleons respectively; $r = (r_1 + r_2)/2$ is a reasonable, although not rigorously tested "local density approximation". The nuclear density (r) for neutron scattering was assumed to be proportional to the proton density obtained from electron

scattering. For heavier nuclei (A > 100), calculations were done also assuming a "neutron skin" with about 2.6% increase in the neutron rms radius over the one of the proton, but the results were not sentitively different for the energy of these measurements. This is not the case for proton scattering where it has been shown[6] that by introducing a neutron skin in the calculations the agreement with the measurements is improved. The effective interaction g(r) is complex, radial, density and energy dependent. Only the central potential has been calculated following the JLM[2] and BR[3] procedures and details of these calculations can be found in Ref. 7. The effective interaction used in the calculation of the spin-orbit potential has been taken from the work of Bertsch et al.[8] (Elliot matrix elements).

The predictions of the MOP were compared with the elastic angular distribution data. The real and imaginary terms of the central potential were multiplied by normalyzing constants λ_V and λ_W respectively. These parameters, which are the only ones used in the calculations, were adjusted by least squares for an optimal fit to the data. In Table I are listed their values together with the values of χ^2/N obtained from the JLM and BR calculations. It can be seen that for the real central potential, the value of λ_V is close to unity for all the values of A in both calculations. This indicates that the volume integrals are correctly predicted in both models. The normalizing constants λ_W for the imaginary potential show more scatter than those for the real potential (specially the values for the BR potential), although they have a definite decreasing trend with energy. The overall agreement found between the MOP calculations after normalization and the measurements is reasonably good, with the JLM potential giving a better representation of the data over the entire mass range. In Figs. 2-4 (solid lines) the latter calculations are compared with the data.

B. Phenomenological calculations. In addition to the comparison with the microscopic potentials, the data have been compared with calculations carried out with phenomenological optical model potentials (OMP) for two global parameter sets optimized for neutron data, the Becchetti-Greenlees[8] and the Rapaport et al.[9] global potentials. The results obtained with these two sets are quite similar, with the Rappaport et al. (the "Ohio set") giving slightly better agreement with the measurements. Accordingly, only the OM calculations performed with the parameters given in Ref. 9 for the set A, E < 15 MeV will be reported. Following the same normalizing procedure used for the MOP, the strengths of the real and imaginary terms of the central potential were adjusted to optimize the fits to the data. The values found for the normalizing parameters λ_V and λ_W, which correspond to the ratios between the values of V_R and W_D after the search and their initial values[9], are listed in Table I. The agreement between the calculations with the "Ohio set" and the data are quite close to the results obtained with the JLM potential as can be seen in Figs. 2-4 (dashed lines). The values of χ^2/N obtained with this global set are listed in Table I. They are similar to those obtained with the JLM calculation, while the values obtained with the BR potential are 2 to 3 times larger than either one of the above potentials.

With the exception of the light nuclei Be and C, both calculations reproduce rather well the measurements. It has been shown[10] that the failure of the calculations to fit the angular distributions at the backward angles for these two nuclei results mainly from their strongly deformed nature, which has not been accounted for in the present calculations.

Actinide Targets

The ^{232}Th, ^{238}U and $^{239}Pu(n,n)$ elastic angular distributions were measured at 14.1 MeV. Because these targets are characterized by large and permanent quadrupole (P_2) and hexadecapole (P_4) nuclear deformations, coupled channel (CC) calculations were carried out for both MOP and phenomenological optical model potentials. Levels of the ground state (GS) rotational band up to the 6^+ for Th and U, and up to the $9/2^+$ for Pu have been included in the calculations.

The microscopic calculations have been done by folding the JLM effective interaction with the deformed GS nuclear density

$$\rho(r) = \sum_{\lambda=0}^{8} \rho_\lambda(r) Y_{\lambda 0}(\theta) \qquad (2)$$

The Legendre polynomial expansion includes terms up to $L_{max} = 8$. Only the real and imaginary central potential are deformed. The spin orbit potential is real, spherical and independent of energy. Details of these calculations can be found in Ref. 11. The only free parameters are the normalization constants λ_V and λ_W, the effective interaction ranges t_V and t_W included in the real and imaginary potential respectively, and the strength of the spin-orbit potential V_S. The values of these last three parameters are $t_V = 1.2$ fm, $t_W = 1.3$ fm and $V_S = 50$ MeV - fm^5. They were obtained from the analysis of neutron and proton scattering cross sections for ^{208}Pb. In Fig. 5 is shown the comparison between the calculations (solid lines) and the data. The agreement is quite reasonable given that the normalization constants $\lambda_V = 0.94$ and $\lambda_W = 0.82$ are the only two parameters optimized in the present calculation.

CC calculations with the global potential of Klepalskij et al.[12] have also been done. The optical parameters used in these calculations are those prescribed by the set, since this potential has been optimized[12] for the actinide region in the energy region of a few keV to 15 MeV. In other words, the normalization constants λ_V and λ_W are both equal to 1 for this calculation. The calculated differential cross sections are shown in Fig. 5 by the dotted lines. The good agreement found with the measurements is not surprising since phenomenological global potentials have as many as nine available parameters to optimize the fits in for a given mass and energy region.

INTEGRAL NEUTRON MEASUREMENTS

OBJECTIVE

The optimum design of fusion, fusion-fission hybrid reactors requires calculations that accurately describe the interaction of 14 MeV neutrons with the materials present in the design. The value of such studies depends in large measure on the accuracy of the codes and cross sections used in calculating the design parameters of the reactor concepts. Codes and evaluated cross sections can be checked directly against measurements of the neutron- and gamma-emission spectra from simple geometrical assemblies (spherical targets) and individual isotope materials.

Under the Pulsed Sphere Program (PSP), we have measured the neutron and gamma spectra emitted by many materials from lithium to plutonium bombarded with 14 MeV neutrons. From the comparison of these measurements with calculations using evaluated neutron and photon cross sections, many problems

have been unfolded[13-15] related to the magnitude and representation of the cross sections in the libraries. In Ref. 16 can be found a tabulation of all the measured spherical assemblies under this program.

EXPERIMENTAL METHOD

Measurements of the neutron emission spectra have been made using the sphere transmision and TOF techniques[17]. The 14 MeV nominal energy neutrons from the $^{3}H(d,n)^{4}He$ reaction are generated using the 400-keV $^{2}H^{+}$ beam from the LLNL insulated-core-transformer (ICT) accelerator. The beam, swept at a 0.5 MHz rate and bunched to <2 ns burst width, strikes a tritium-loaded titanium target mounted at the end of a low mass conical assembly. The titanium which absorbs the tritium is 1.59 cm in diameter and 4 mg/cm^{2} thick and is evaporated on a 0.076 cm thick tungsten backing. Details on the geometry and composition of the low mass assembly can be found in Ref. 17. The 14 MeV neutron production at the tritium target is monitored by counting the associated alpha particle with a thin (25 m) silicon surface-barrier detector. This detector is mounted on the conical assembly at about 35 cm from the tritium target and at a 174 angle from the $^{2}H^{+}$ beam line. A schematic representation of the experimental set up is shown in Fig. 6.

The detectors used in the measurements of the neutron ($1 < En < 15$ MeV) and gamma leakage spectra are NE213 and stilbene scintillators. For neutron energies from 1 MeV to below 1 eV, a ^{6}Li scintillator is used. Measurements of the relative and absolute efficiency of these detectors have been discussed in detail elsewhere.[18,19]

Calculations have been carried out with the code TART, a coupled neutron-photon Monte Carlo transport code[20]. The variations in energy and intensity with angle of the of the 14 MeV neutron source, the time spread of the deuteron beam from the ICT accelerator and the geometry and composition of the low-mass tritium target assembly are included in the calculations. The validity of the representations of these elements in the calculational model can be inferred from the excellent agreement between calculations and measurements for a "Blank" run[14]. A "Blank" run is by definition a meusurement of the TOF spectrum with the spherical assembly removed (see Fig. 6). These runs, which alternate with those taken with the sphere in place, are used for time indepedent background corrections and source strength determination.

The TART code tabulates the energy and time-of-arrival of each neutron at the detector position. Folding in the detector efficiency as a function of neutron energy yields a calculated time-of-arrival neutron count spectrum which can be directly compared with the measured TOF spectrum. The transformation from measured time-of-arrival spectra to energy spectra is strictly valid only for small spheres and non-multiplying assemblies. The error introduced in the transformation can be ascertained by transforming the calculated time-of-arrival spectra to energy spectra and comparing directly with the Monte Carlo calculations of the energy spectra.

Extensive tests of cross sections evaluations for 14 MeV neutrons for materials of interest to the fusion and shielding communities has been done under the Pulsed Sphere Program during the last fifteen years. The neutron leakage spectra from spherical assemblies (thicknesses varying between 1 and 5 mean free paths, mfp, for 14 MeV neutrons) have been measured for over 30 materials[16]. These measurements have been compared with the Monte Carlo calculations as described above, using the ENDF/B files[21]. Versions III, IV and V of this library have been used during the years as updating of the cross sections between succeeding versions has taken place. Calculations have also been done with the Livermore evaluated neutron and photon libraries, ENDL[22]. Because most of the results can be found in the published literature (see list of publications in Ref. 16), only the last set of measurements and calculations[19] will be presented here.

Recently we have measured the emission spectra from Holmium (0.8 mfp), Tantalum (1 and 3 mfp), Gold (1.9 mfp), and Lead (1.0 mfp). Lead is of special interest since it has been proposed as a neutron multiplier in some conceptual designs of fusion blankets. These elements were chosen to cover a wide range of heavy nuclei characterized by different nuclear structure as a result of their shape and closure of neutron and proton shells. Holmium and tantalum are strongly deformed nuclei, while gold and lead are spherical nuclei. In addition, in lead both neutron and proton shells are closed for the isotope of greatest abundance. We have measured the neutron leakage spectra in the energy region of 1 to 15 MeV and the results have been compared with the predictions of the Monte Carlo calculations using the ENDF/B-V and ENDL neutron cross sections libraries. ENDF/B-V contains independent

evaluations only for gold and lead; it does not have an evaluation for holmium and the one for tantalum is from an earlier ENDL evaluation which presently has been superseded. In addition to these two evaluated libraries, a test library ($ALICE_{Sph}$) based on the ENDL was generated in which the code[23] ALICE/LIVERMORE 82 was used. This code provided substitute differential data for reaction cross sections and spectra for (n,n') continium, (n,2n), (n,3n), (n,p), (n,n'p + n,pn'), (n,α) and (n,n'α+n,αn') reactions for incident neutron energies between 2.0 and 20.0 MeV. The single and multiple particle emission are calculated from evaporation processes[24] and precompound decay using the hybrid/geometry dependent hybrid models[25]. In Fig. 7 are shown the comparisons between the measured TOF spectrum for the 1 mfp Ta sphere and the TART calculations with the ENDF/B-V, ENDL and $ALICE_{Sph}$ cross section libraries. From the agreement obtained it can be concluded that the calculation with $ALICE_{Sph}$ (bottom curve) gives an overall better representation of the measurements. This is quantitatively shown in Table II, where the measured integrals for three energy intervals 1-5, 5-10, and 10-15 MeV intervals are given together with the ratios of the calculated/measured integrals obtained from each calculation for these energy intervals.

The sensitivity of the pulsed sphere data to deformation effects arising from the nuclear shape in the calculated emission spectra was also investigated. A second test library ($ALICE_{CCh}$) was generated where the ENDL elastic and inelastic neutron cross sections to low excited levels in the $ALICE_{Sph}$ library were replaced by those obtained from a coupled channel calculation. These calculations were carried out with the code ECIS79 written by Raynal[26], using global optical potentials optimized for neutron scattering[9]. The values of the ratios - calculated/measured - for the above energy intervals obtained with the $ALICE_{CCh}$ test library are listed in the

last column of Table II. For both the 1 and 3 mfp Ta spheres, the calculations carried out with $ALICE_{CCh}$ show a small improvement in the region of 5 to 15 MeV. All four calculations overestimate the production of neutrons in the 1-5 MeV interval. The evaluated libraries overpredict the production of neutrons in this energy interval by as much as 20-30 % and ALICE does it by 15-20%. This effect seems to result mainly from the shape of the energy differential spectrum predicted for the secondary neutrons. A comparison[19] with the measurements of the neutron differential spectrum at 14.1 MeV by Vonach et al.[27], and at 14.6 MeV Hermsdorf et al.[28], has also shown that the above calculations overestimate the measured spectra in the region of 2 to 5 MeV. For a detailed discussion of these results and those obtained for Ho, Au and Pb, see Ref. 19.

In order to facilitate the comparison of the present measurements with calculations carried out elsewhere, the measured TOF spectra of the emitted neutrons have been transformed[17] to energy spectra by calculating the energy relativistically from the time of arrival t_i of the neutrons.

$$E_i = 939.6\ ([1 - (L/t_i c)^2]^{-1/2} - 1) \qquad (3)$$

Where L is the distance from the center of the sphere to the face of the detector. Unfolding the detector efficiency from the time spectra and using the differential energy spectrum for the source neutrons, the energy spectrum is obtained from the above formula in units of neutrons per MeV per 14 MeV source neutron (Table III).

SUMMARY

In this paper the 14 MeV neutron work done at LLNL, has been discussed, which covers neutron time-of-flight measurements and calculations of (1), differential cross sections, and (2), of the integral leakage neutron and gamma-ray spectra. The materials studied coverd a wide mass range, ^{9}Be to ^{239}Pu, and are found in the conceptual design of fusion reactors.

The calculational analysis of the differential data[1] have been done using microscopic optical potentials derived from the treatment of Jeukenne, Lejeune, and Mahaux[2] (JLM), and of Brieva and Rook[3] (BR). The agreement with the measured angular distributions is better[1] for the JLM potentials than for the BR. The latter overestimates systematically the forward angle cross sections and the total cross sections[1]. These effects are associated[7] with the pronounced deviation of the BR potentials from the Woods-Saxon shape. The microscopic calculations with the JLM potentials also compare quite favorably with calculations using global[9] optical model potentials, giving in some cases better fits to the data. Only two normalizing parameters, λ_V and λ_W, have been used in these calculations. Their values (Table I) have been obtained by adjusting the real and imaginary parts of the central potential by a least squares procedure to optimize the fits to the data. The required normalizing parameters are within a few percent of unity in all cases for the real potential. The values of λ_W for the imaginary potential exhibits a mass variation that is most pronounced for the BR potentials. The values for the JLM and "Ohio" potentials are closer to constant values (0.96 0.15 and 0.84 0.10 respectively).

The integral data have been compared[16] with Monte Carlo calculations carried out with the code TART[20], using the evaluated libraries ENDF/B-V

(versions III and IV have also been tested in the past) and ENDL. The most recent measurements[19] for Ho, Ta, Au and Pb have also been compared with calculations done with two "test neutron libraries", $ALICE_{Sph}$ and $ALICE_{CCh}$, obtained by modifying the ENDL library. In the first, the precompound, compound and reaction cross sections have been obtained from nuclear model calculations using the code[23] ALICE/LIVERMORE 82. In the second test library we have substituted in ENDL, in addition to the above cross sections, the elastic and inelastic to low-lying levels cross sections. These cross sections have been generated by coupled channel calculations done with the code[26] ECIS 79, in order to account for the strong rotational (Ho and Ta) and vibrational (Au and Pb) nature of the targets.

From the comparisons of the calculated TOF with the data the following conclusions can be extracted: 1) From the two evaluated libraries, ENDL gives consistently better agreement with the measurements than the ENDF/B-V (see Ref. 19). 2) The test libraries give surprisingly good agreement with the data. The attractive feature of libraries is that only default parameters are used in the calculations, which have been obtained from the use of precompound and compound nuclear models[24,25] and global optical potentials[9] over a wide range of mass and energy. 3) The introduction of collective effects ($ALICE_{CCh}$) results in a modest improvement in the agreement with the data in the 1.0 to 10 MeV interval. However, collective effects are very important in the analysis of differential scattering cross sections from deformed nuclei[10], where a noticeable improvement is obtained in the fits of the optical model calculations to the measured angular distributions at the backward angles.

ACKNOWLEDGEMENTS

The work that I have summarized in this paper represents the collaboration of many people during the years. I would like to thank here those whose contributions have been essential to the success of these programs, including C. Wong, B. A. Pohl, T. T. Komoto, F. S. Dietrich, and R. C. Haight. This work was performed under the auspices of the U.S. Department of Energy by Lawrence Livermore National Laboratory under Contract # W-7405-Eng-48.

FIGURE CAPTIONS

Fig. 1 Schematic representation of the Livermore time-of-flight facility and wedge shielding used in the present measurements.

Fig. 2 Measurements of the neutron elastic differential cross sections for ^{9}Be, C, ^{27}Al and ^{59}Co. Calculations carried out with the microscopic optical potentials of Jeukenne, Lejeune and Majaux (JLM: solid lines) and the global potential of Rapaport et al. (dashed lines). For C and Fe the calculations have been done assuming 100% ^{12}C and ^{56}Fe isotopic composition respectively.

Fig. 3 Measurements of the neutron elastic differential cross sections for ^{89}Y, ^{93}Nb, In and ^{140}Ce. Calculations as in Fig. 1.

Fig. 4 Measurements of the neutron elastic differential cross sections for ^{181}Ta, ^{197}Au, ^{208}Pb and ^{209}Bi. Calculations as in Fig. 1.

Fig. 5 Measurements of the neutron elastic differential cross sections for ^{232}Th, ^{238}U and ^{239}Pu. Calculations carried out with deformed semi-microscopic optical potentials (JLM: solid lines) and the global potential of Klepatskij et al. (dashed lines)

Fig. 6 Schematic representation of the experimental set up for the Pulsed Sphere measurements. In the insert is shown the spherical target geometry.

Fig. 7 Comparison of measured (xxx) and calculated (---) neutron TOF spectra for 1.0 mfp ^{181}Ta. The calculations have been carried out with the ENDF/B-V (upper curve), ENDL (middle curve), and $ALICE_{Sph}$ (bottom curve) libraries.

Table I. Values of χ^2/N and the normalization parameters λ_V and λ_W for the neutron elastic differential cross sections at 14.6 MeV, compared with the Brieva-Rook and JLM microscopic optical model potentials, and with the Rapaport *et al.* "Set A" global potential.

	Brieva-Rook			J L M			Rapaport *et al.*		
Target	χ^2/N	λ_V	λ_W	χ^2/N	λ_V	λ_W	χ^2/N	λ_V	λ_W
Be	46.4	0.94	1.23	29.4	1.00	1.25	40.2	0.96	0.83
C	60.3	1.03	1.59	14.1	1.04	1.04	32.5	0.96	0.67
Al	51.1	1.02	1.68	6.3	0.99	1.06	12.0	0.96	0.72
Fe	13.0	1.04	1.52	3.9	0.96	0.97	4.0	1.00	0.78
Co	32.8	1.02	1.48	2.6	0.95	0.96	6.7	0.98	0.82
Y	38.5	1.02	1.08	5.5	0.97	0.92	8.00	1.00	0.84
Nb	9.6	1.02	1.28	2.0	0.96	0.94	2.2	0.98	0.96
In	12.7	1.00	1.51	7.2	0.98	1.18	7.6	1.00	1.07
Ce	12.9	1.01	1.19	7.6	0.97	0.92	7.5	1.02	0.84
Ta	24.9	0.99	0.98	6.8	0.94	0.70	6.5	0.99	0.87
Au	7.4	1.00	1.00	7.6	0.98	1.00	3.1	0.99	0.92
Pb	11.0	1.01	0.97	4.0	0.97	0.81	2.9	1.00	0.84
Bi	17.6	1.01	0.92	8.2	0.97	0.80	6.4	1.00	0.82

Table II Measured integrals* for 1.0 and 3.0 mfp Ta and ratios of calculated-to measured integrals

#mfp	ΔE [MeV]	Experiment* ±5%	R(ENDF/B-V)	R(ENDL)	$R(ALICE_{Sph}$	$R(ALICE)_{CCh}$
1	1.- 5.	0.256	1.281	1.230	1.152	1.148
	5.-10.	0.024	0.975	1.107	1.045	0.984
	10.-15.	0.618	1.047	1.024	1.071	1.083
	1.-15.	0.898	1.115	1.088	1.096	1.102
3	1.- 5.	0.316	1.259	1.266	1.196	1.209
	5.0-10	0.027	0.970	1.118	0.908	0.930
	10.-15.	0.278	0.860	0.813	0.950	0.971
	1.-15.	0.621	1.068	1.056	1.074	1.090

*In units of neutron counts (sphere in) divided by the total number of 14 MeV source counts (sphere out). The error in the ratios is also 5%.

Table III. Neutrons/MeV-Source neutron calculated from the measured neutron time-of-flight spectra.

ΔE[1 MeV]	Ho [1 mfp] $\times 10^{-3}$	Ta [1 mfp] $\times 10^{-3}$	Ta [3 mfp] $\times 10^{-3}$	Au [2 mfp] $\times 10^{-3}$	Pb [1 mfp] $\times 10^{-3}$
1 - 2	6.504	7.284	10.397	13.000	12.830
2 - 3	2.902	2.937	3.141	4.587	7.462
3 - 4	1.208	1.239	1.290	1.863	2.992
4 - 5	0.606	0.615	0.670	0.897	1.294
5 - 6	0.382	0.395	0.429	0.527	0.636
6 - 7	0.343	0.355	0.398	0.460	0.471
7 - 8	0.285	0.295	0.332	0.382	0.367
8 - 9	0.272	0.290	0.330	0.382	0.397
9 - 10	0.274	0.309	0.346	0.401	0.437
10 - 11	0.274	0.320	0.355	0.379	0.393
11 - 12	0.286	0.323	0.320	0.354	0.330
12 - 13	0.411	0.428	0.313	0.382	0.375
13 - 14	1.026	1.194	0.674	0.805	0.852
14 - 15	53.797	45.127	19.690	29.559	48.727

REFERENCES

1. L. F. Hansen, F.S. Dietrich, C. H. Poppe, and C. Wong. Phys. Rev. C 31, 111 (1985). (See Refs. 1-36)
2. J. P. Jeukenne, A. Lejeune, and C. Mahaux, Phys. Rev. C 16, 80 (1977).
3. F. A. Brieva and J. R. Rook, Nucl. Phys. A291, 299 (1977); A291, 317 (1977).
4. L. F. Hansen, J. L. Garibaldi, R. Keville, and B. A. Pohl, "Tritium/Deuterium Gas Cell", UCID-20175, Lawrence Livermore National Laboratory (1984).
5. C. Wong, S. M. Grimes, C. H. Poppe, V. R. Brown and V. A. Madsen, Phys. Rev. C 26, 889 (1982). (See Refs. 11 and 12).
6. F. S. Dietrich and F. Petrovich, AIP 124, 90 (1984).
7. S. Mellema, R. W. Finlay, and F. S. Dietrich, Phys. Rev. C 28 (1983).
8. G. Bertsch, J. Borysowicz, H. McManus, and W. G. Love, Nucl. Phys. A284, 399 (1977).
9. J. Rapaport, V. Kulkarni, and R. W. Finlay, Nucl. Phys. A330, 15 (1979).
10. L. F. Hansen, R. C. Haight, B. A. Pohl, and C. Wong, AIP 124, 314 (1984).
11. Ch. Lagrange and M. Girod, J. Phys. G: Nucl. Phys. 9, 97 (1983).
12. A. B. Klepatskij, V. A. Kon'shin, and E. Sh. Sukhovitskij, "The Optical Potential For Heavy Nuclei", INDC(CCP)-161/L (1980).
13. L. F. Hansen, C. Wong, T. T. Komoto, and J. D. Anderson, Nucl. Sci. Eng. 60, 27 (1976).
14. L. F. Hansen, C. Wong, T. T. Komoto, B. A. Pohl, E. Goldberg, R. J. Howerton, and M. Webster, Nucl. Sci. Eng. 72, 35 (1979).
15. L. F. Hansen, C. Wong, T. T. Komoto, B. A. Pohl, and R. J. Howerton, Nucl. Tech. 51, 70 (1980).

16. L. F. Hansen, T. T. Komoto, B. A. Pohl, and C. Wong. "Summary of Measurements and Calculations of Neutron and Gamma-Ray Emission Spectra From Spheres Pulsed With 14 MeV Neutrons", UCID-19604, Lawrence Livermore National Laboratory (1982).

17. C. Wong, J. D. Anderson, P. Brown, L. F. Hansen, J. L. Kammerdiener, C. Logan, and B. A. Pohl, "Livermore Pulsed Sphere Program: Program Summary Through July 1971", UCRL- 51144, Rev. I, Lawrence Livermore National Laboratory (1972)

18. C. Wong, E. F. Plechaty, R. W. Bauer, R. C. Haight, L. F. Hansen, R. J. Howerton, T. T. Komoto, J. D. Perkins, and B. A. Pohl, "Measurements and Calculations of the Leakage Multiplication from Hollow Berylium Spheres", UCRL-91774, Lawrence Livermore National Laboratory (1985).

19. L. F. Hansen, H. M. Blann, R. J. Jowerton, T. T. Komoto, and B. A. Pohl, "The Transport of 14 MeV Neutrons Through Heavy Materials 150 < A < 208", UCRL-92426, Lawrence Livermore National Laboratory (1985).

20. E. F. Plechaty and J. R. Kimlinger, "TART Coupled Neutron-Photon Monte Carlo Transport Code", UCRL-5400, Vol. 14, Lawrence Livermore National Laboratory (1975).

21. ENDF/B Library, Brookhaven National Laboratory.

22. ENDL, Lawrence Livermore Laboratory (LLL) Evaluated Nuclear Data Library. Evaluated by R. J. Howerton et al., UCRL-50400, Vol. 15, Parts A to E (1975-1978).

23. M. Blann and J. Bisplinghoff, "Code ALICE/LIVERMORE 82," UCID-19614 (1982).

24. V. F. Weisskopf and D. H. Ewing, Phys. Rev. 57, 472 (1940).

25. M. Blann, Phys. Rev. Lett. 27, 337 (1971); 28, 757 (1982).

26. J. Raynal, "The Structure of Nuclei". Course on Nuclear Theory given in Triest. Sponsored by the IAE Egency, Vienna (1979).

27. H. Vonach, A. Chalupka, F. Wenninger, G. Staffel, "Measurements of the Angle-Integrated Secondary Neutron Spectra from Interaction of 14 MeV Neutrons With Medium and Heavy Nuclei", BNL-NCS-51245, Vol. I, 343 (1980).

28. D. Hermsdorf, A. Meister, S. Sassonoff, D. Seelinger, K. Seidel and F. Shanin, "Differentielle Neutronemission-querschnitte bei 14.6 MeV Einschubenergie für Die Elemente Be, C, Na, Mg, Al, Si, P, S, Ca, Ti, V, Cr, Mn, Fe, Co, Ni, Cu, Zn, Ga, Se, Br, Zr, Nb, Cd, In, Sn, Sb, I, Ta, W, AU, Hg, Pb, und Bi", INDC(GDR)-2/L (1975).

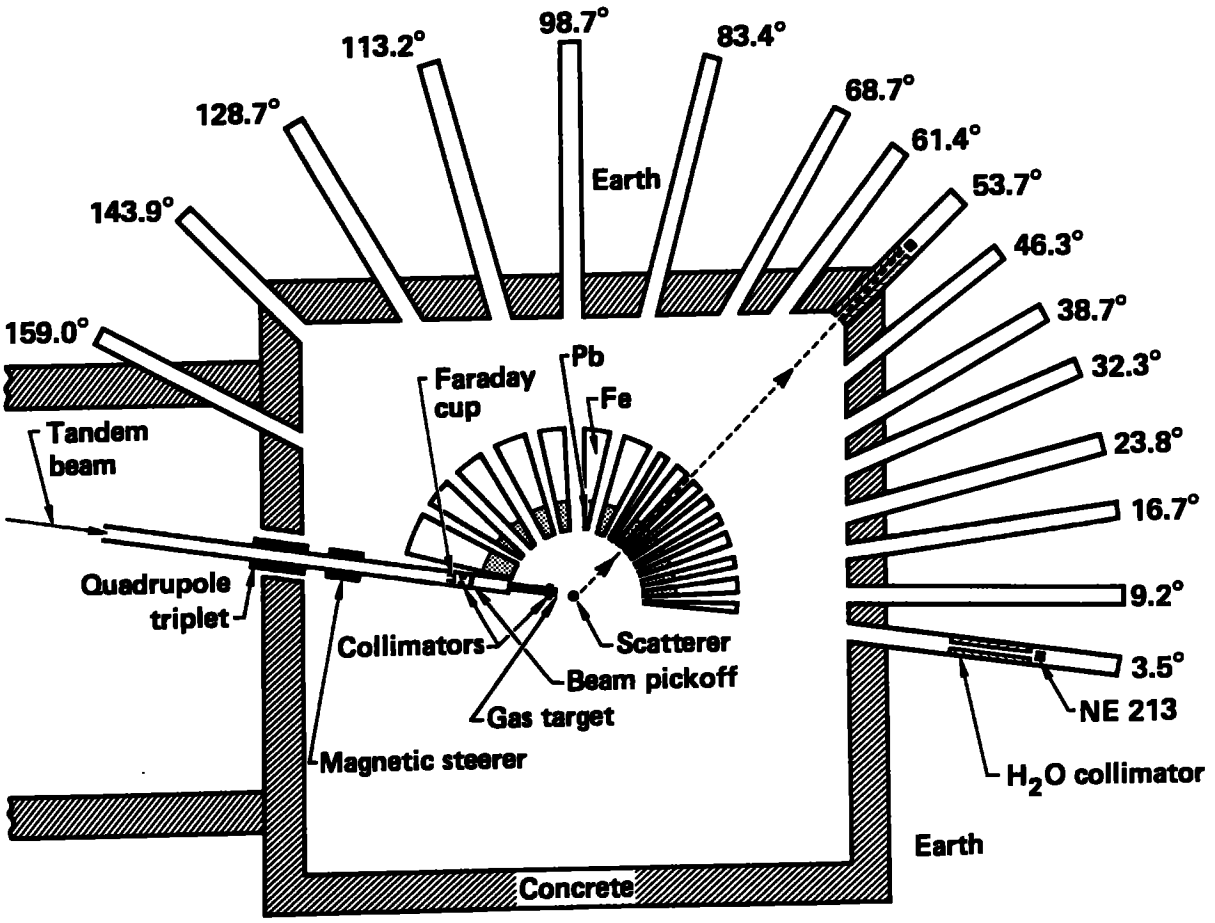
98.7°
113.2°
83.4°
128.7°
68.7°
61.4°
143.9°
Earth
53.7°
46.3°
159.0°
38.7°
Faraday cup
Pb
Fe
32.3°
Tandem beam
23.8°
16.7°
Quadrupole triplet
9.2°
Collimators
Scatterer
3.5°
Beam pickoff
NE 213
Gas target
Magnetic steerer
H_2O collimator
Earth
Concrete

Figure 1

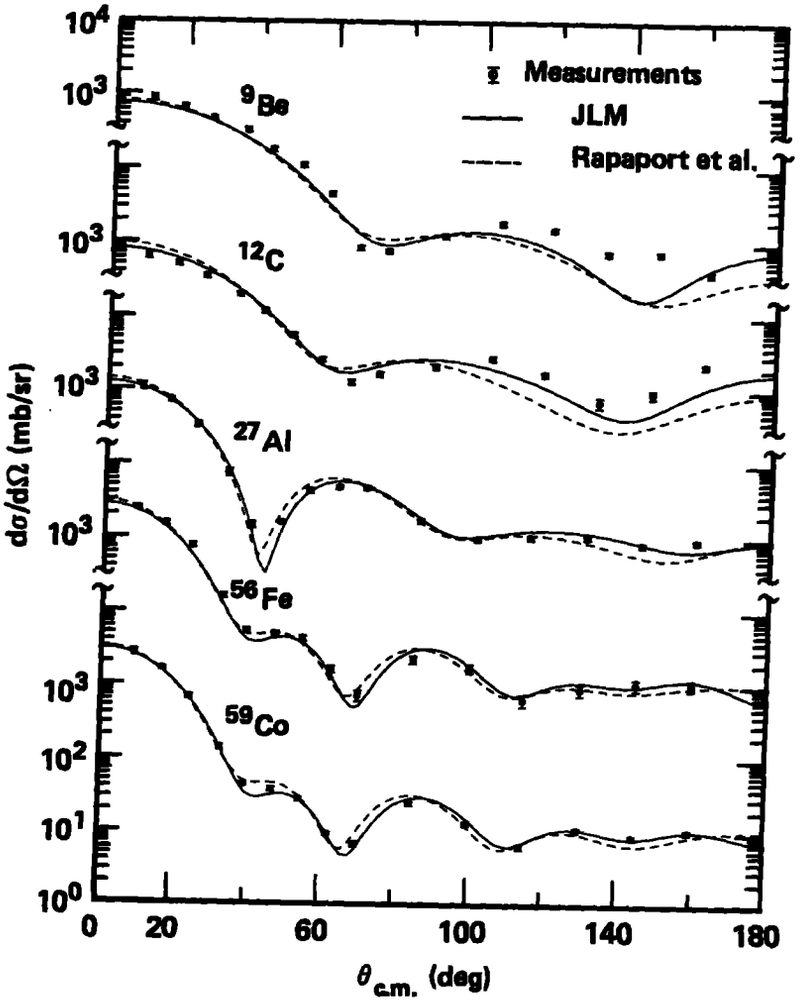
Measurements
JLM
Rapaport et al.
^{9}Be
^{12}C
^{27}Al
^{56}Fe
^{59}Co
dσ/dΩ (mb/sr)
$\theta_{c.m.}$ (deg)
0
20
60
100
140
180

Figure 2

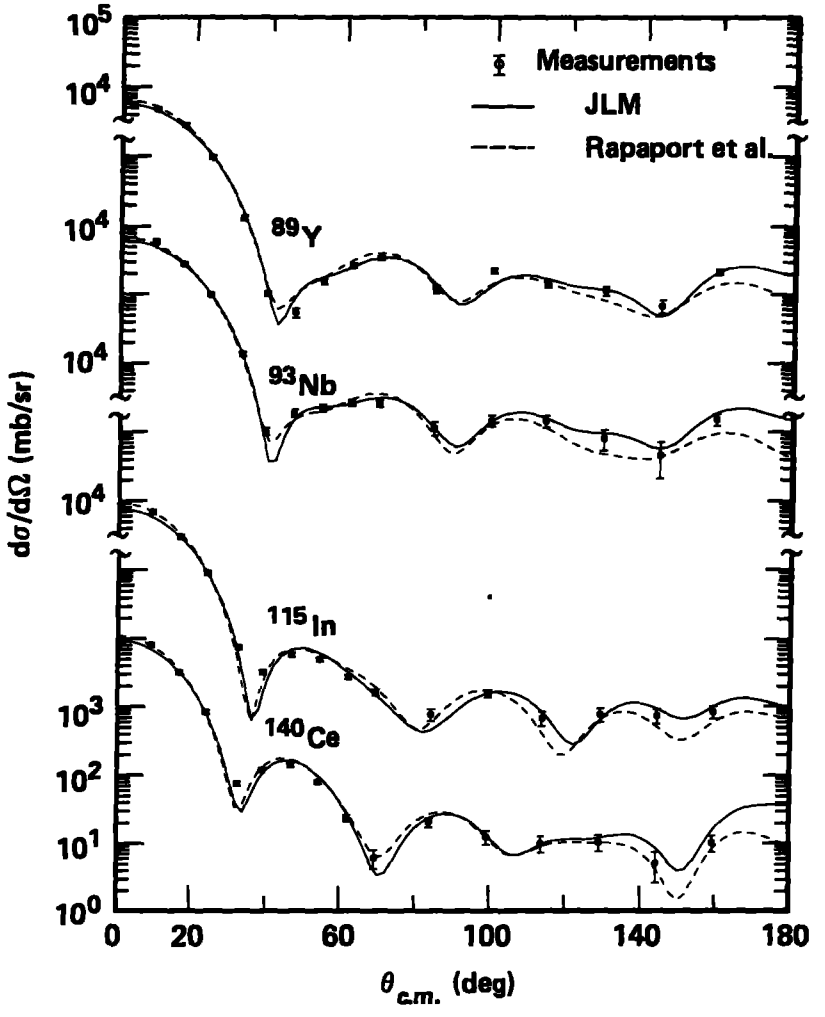
Measurements
JLM
Rapaport et al.
89Y
93Nb
115In
140Ce
dσ/dΩ (mb/sr)
θc.m. (deg)
10^5
10^4
10^4
10^4
10^4
10^3
10^2
10^1
10^0
0
20
60
100
140
180

Figure 3

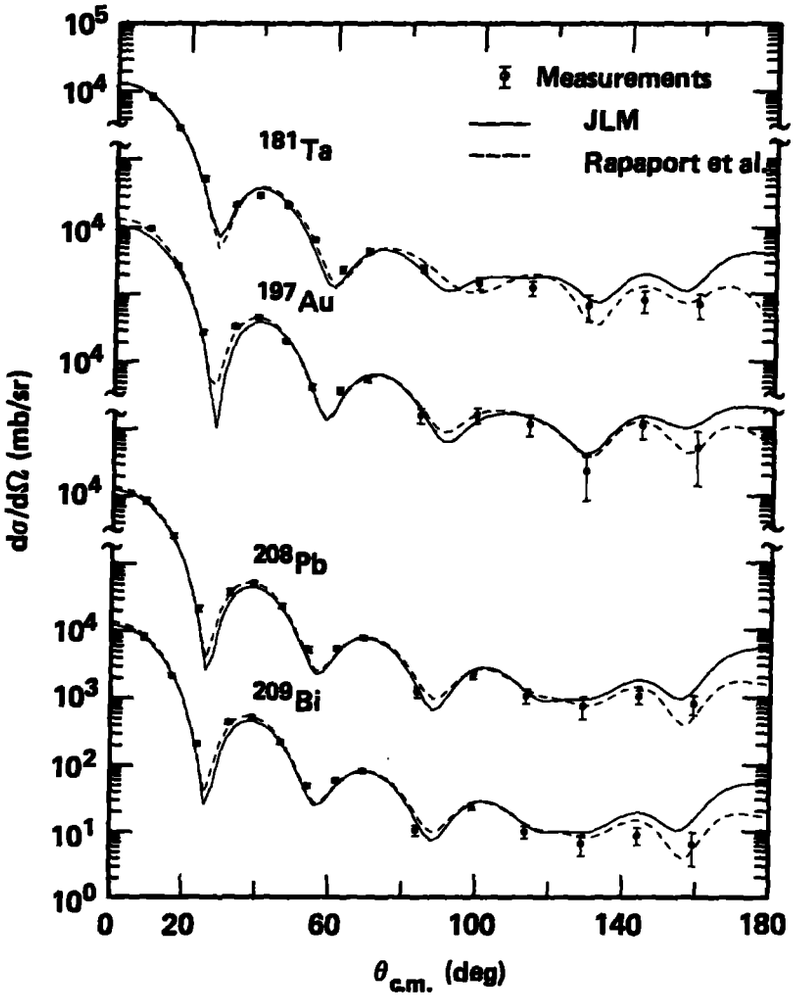
Measurements
JLM
Rapaport et al.
181Ta
197Au
208Pb
209Bi
dσ/dΩ (mb/sr)
θc.m. (deg)
0
20
60
100
140
180

Figure 4

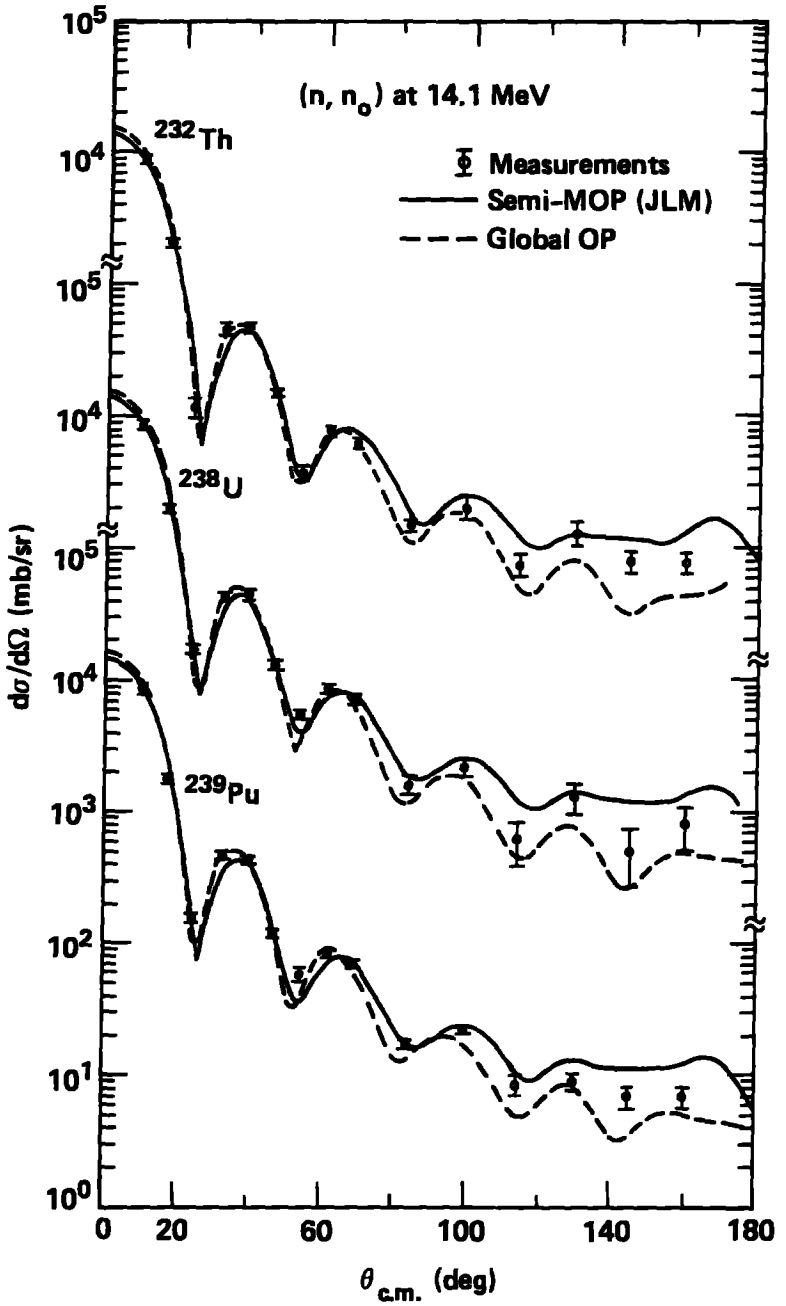
(n, n$_o$) at 14.1 MeV
^{232}Th
^{238}U
^{239}Pu
Measurements
Semi-MOP (JLM)
Global OP
dσ/dΩ (mb/sr)
$\theta_{c.m.}$ (deg)
10^5
10^4
10^3
10^2
10^1
10^0
0
20
60
100
140
180

Figure 5

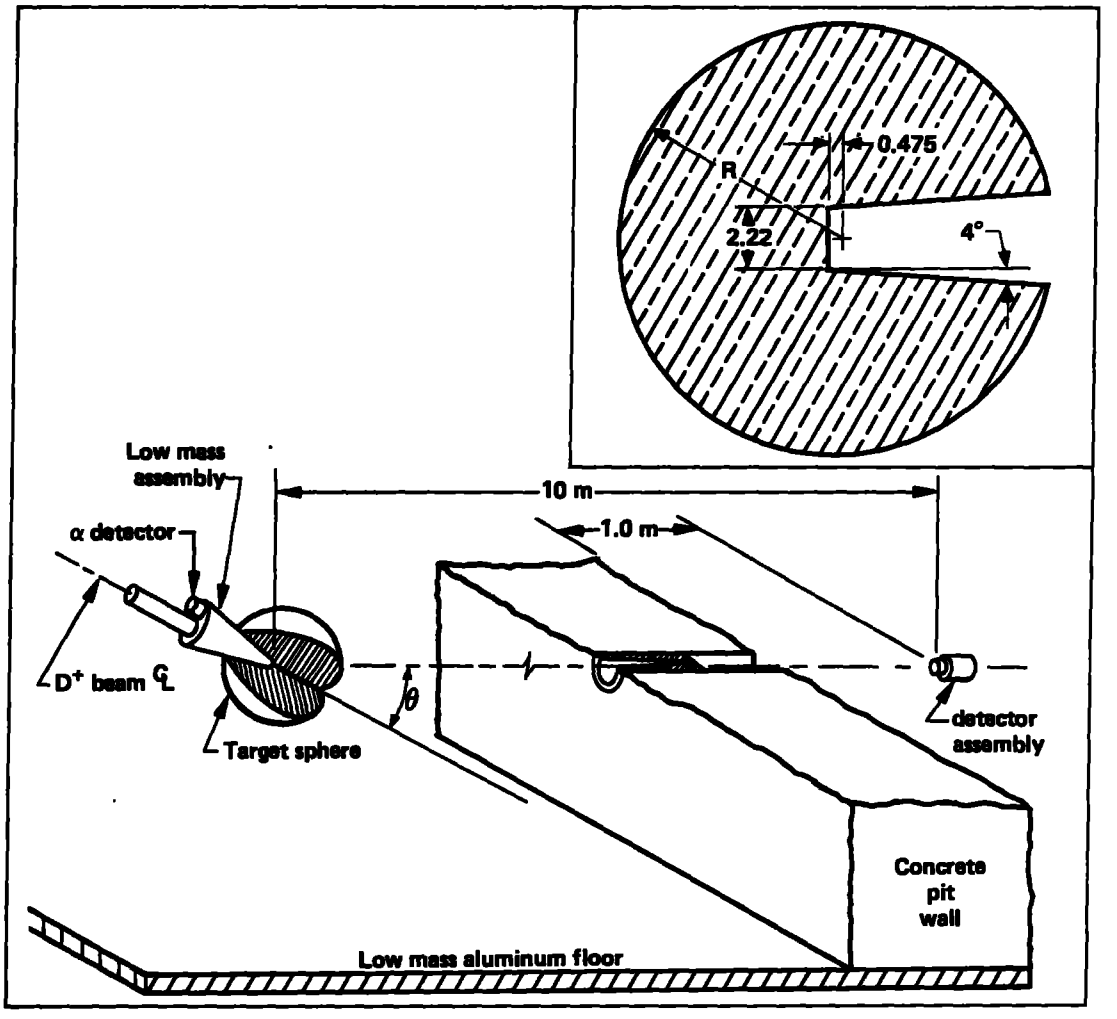
R
0.475
2.22
4°
Low mass assembly
α detector
10 m
1.0 m
D+ beam ℄
Target sphere
θ
detector assembly
Concrete pit wall
Low mass aluminum floor

Figure 6

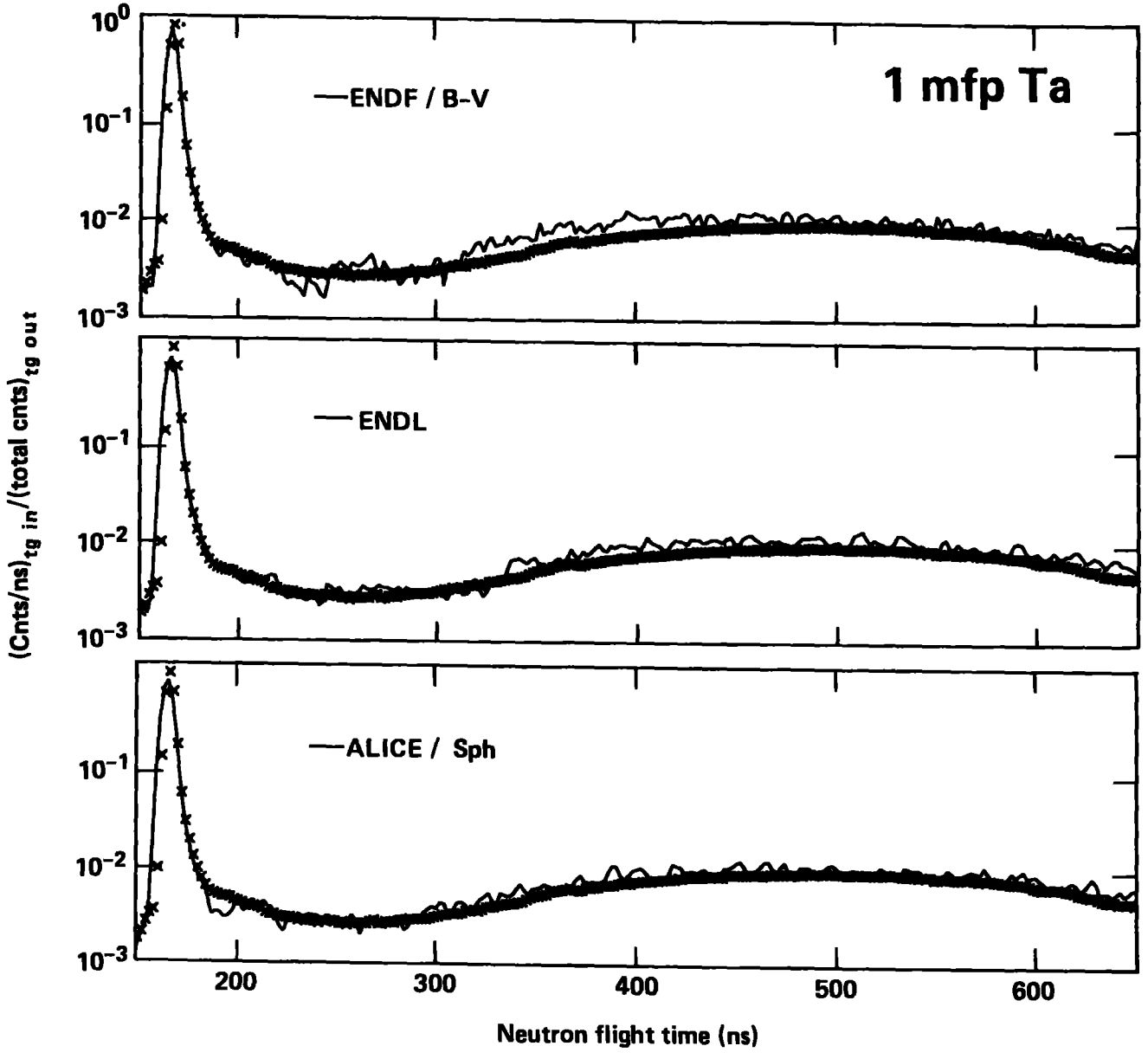
1 mfp Ta
—ENDF / B-V
— ENDL
—ALICE / Sph
10^0
10^{-1}
10^{-2}
10^{-3}
200
300
400
500
600
$(Cnts/ns)_{tg\ in}/(total\ cnts)_{tg\ out}$
Neutron flight time (ns)

Figure 7